

# Structure of an integral membrane sterol reductase from *Methylobacterium alcaliphilum*

Xiaochun Li<sup>1</sup>, Rita Roberti<sup>2</sup> & Günter Blobel<sup>1</sup>

**Sterols are essential biological molecules in the majority of life forms. Sterol reductases<sup>1</sup> including  $\Delta^{14}$ -sterol reductase (C14SR, also known as TM7SF2), 7-dehydrocholesterol reductase (DHCR7) and 24-dehydrocholesterol reductase (DHCR24) reduce specific carbon-carbon double bonds of the sterol moiety using a reducing cofactor during sterol biosynthesis. Lamin B receptor<sup>2</sup> (LBR), an integral inner nuclear membrane protein, also contains a functional C14SR domain. Here we report the crystal structure of a  $\Delta^{14}$ -sterol reductase (MaSR1) from the methanotrophic bacterium *Methylobacterium alcaliphilum* 20Z (a homologue of human C14SR, LBR and DHCR7) with the cofactor NADPH. The enzyme contains ten transmembrane segments (TM1–10). Its catalytic domain comprises the carboxy-terminal half (containing TM6–10) and envelops two interconnected pockets, one of which faces the cytoplasm and houses NADPH, while the other one is accessible from the lipid bilayer. Comparison with a soluble steroid 5 $\beta$ -reductase structure<sup>3</sup> suggests that the reducing end of NADPH meets the sterol substrate at the juncture of the two pockets. A sterol reductase activity assay proves that MaSR1 can reduce the double bond of a cholesterol biosynthetic intermediate, demonstrating functional conservation to human C14SR. Therefore, our structure as a prototype of integral membrane sterol reductases provides molecular insight into mutations in DHCR7 and LBR for inborn human diseases.**

Sterols, amphipathic molecules, are widespread in animals, plants, fungi and some prokaryotes and a large variety exist<sup>4</sup>, including ergosterol, hopanoids, phytosterol and cholesterol. The most abundant sterol in animals is cholesterol, which not only has a vital role in the maintenance of membrane strength and permeability, but also serves as a precursor for the biosynthesis of steroid hormones<sup>5,6</sup>. Endogenous biosynthesis is the major source of sterols, and the biosynthetic pathway from water-soluble small metabolites via intermediates of increasing complexity up to water-insoluble sterols encompasses numerous distinct enzymes<sup>1,7</sup>, many of which contain multiple transmembrane segments. To date, no structure of the integral membrane enzymes involving sterol biosynthesis has been determined. Sterol reductases<sup>1</sup>, integral membrane enzymes including C14SR, DHCR7 and DHCR24, can reduce specific carbon-carbon double bonds of the sterol moiety using a reducing cofactor at distinct steps in sterol and cholesterol biosynthesis (Extended Data Fig. 1).

Curiously, the multifunctional lamin B receptor<sup>2</sup> (LBR), located in the inner nuclear envelope membrane, also contains a domain in its C-terminal portion that is highly homologous to human sterol reductase<sup>8</sup> (Extended Data Fig. 2). Indeed, complementary DNA of human LBR complements reductase gene (*ERG24*) deletion in yeast, supporting the idea that LBR can substitute for sterol reductase activity<sup>9</sup>. Mutations in LBR and DHCR7 lead to various human genetic diseases<sup>1</sup> (Pelger–Huët anomaly<sup>10</sup> (PHA) and Greenberg skeletal dysplasia<sup>11</sup> (also known as hypodysplastic calcification-moth-eaten skeletal dysplasia, HEM) related to LBR; and Smith–Lemli–Opitz syndrome<sup>12,13</sup> (SLOS) related to DHCR7). However, structural knowledge of these important membrane-embedded

enzymes is lacking, and therefore a mechanistic understanding cannot be developed.

To gain more insight into sterol reductases, we set out to determine the crystal structure of one of its family members. In screening for crystal-forming representatives of integral membrane sterol reductases, we found a homologue from the methanotrophic bacterium *Methylobacterium alcaliphilum* 20Z, MaSR1, which shares 38–45% sequence identity and 51–62% similarity to human C14SR, DHCR7 and the C-terminal portion of LBR (Extended Data Fig. 2). *Methylobacterium alcaliphilum* 20Z is an aerobic methanotroph, the cell membrane of which contains significant levels of sterols and hopanoids<sup>14</sup>.

Expression of MaSR1 complements the deletion of the  $\Delta^{14}$ -sterol reductase gene (*ERG24*) in yeast, indicating that MaSR1 is a bona fide sterol reductase (Extended Data Fig. 3, lanes 1–3). To test whether MaSR1 can function in human cholesterol biosynthesis, we performed the sterol reductase activity assay of MaSR1 after expression in human HEK293 cells and employed 5 $\alpha$ -cholesta-8,14-dien-3 $\beta$ -ol (C27 $\Delta^{8,14}$ ), a human cholesterol biosynthetic intermediate analogue<sup>15–17</sup> of 4,4-dimethylcholesta-8,14-dien-3 $\beta$ -ol (C29 $\Delta^{8,14}$ , Extended Data Fig. 1), as the substrate (Fig. 1a). This assay has been used for initial identification<sup>15</sup> and further investigation<sup>16,17</sup> of mammalian sterol reductases. The catalytic efficiency of MaSR1 is about 75% of that of human C14SR (Fig. 1b, c). We conclude that MaSR1 can function like human C14SR and specifically reduce the double bond of the approximate cholesterol biosynthetic intermediate.

We crystallized MaSR1 in space group *P1* with NADPH. The diffraction of the crystal is anisotropic (Methods and Extended Data Fig. 4). The structure was determined by selenium-based single-wavelength anomalous dispersion and refined at 2.74 Å resolution (Extended Data Tables 1 and 2). Introduction of additional selenium anomalous scatterers by selective mutation and preparation of platinum derivatives confirmed that the atomic model was correct (Extended Data Fig. 5 and Extended Data Table 3).

Two MaSR1 molecules (rotated by 180°) pack into a crystallographic dimer that forms the asymmetric unit. The dimensions of the MaSR1 monomer are 50 × 45 × 58 Å. The enzyme contains ten transmembrane helices (TM1–10). On the basis of the ‘positive inside rule’ for membrane proteins<sup>18</sup>, we assigned the amino and carboxy termini to face the cytoplasm, consistent with the biochemically determined topology of the yeast homologue Erg24 (ref. 19). There are two short anti-parallel  $\beta$ -sheet regions ( $\beta$ 1–4) interspersed in the cytoplasm-exposed loops as well as two short  $\alpha$ -helices, designated  $\alpha$ 1 and  $\alpha$ 2 (Fig. 2a and Extended Data Fig. 2). Residues 1–23 and 162–176 (part of the loop between TM4 and TM5) are not visible in the electron density map and therefore presumed to be disordered. The binding pocket for NADPH was localized to the C-terminal domain (TM6–10) and a cavity with an unidentified ligand density facing the lipid bilayer is surrounded by TM7 and TM10 (Fig. 2b, c).

Except for the nicotinamide-ribose moiety, the remainder of the NADPH molecule could be clearly identified (Extended Data Fig. 6a, b). The nicotinamide ring is the hydrogen donor in the transient interaction

<sup>1</sup>Laboratory of Cell Biology, Howard Hughes Medical Institute, The Rockefeller University, New York, New York 10065, USA. <sup>2</sup>Department of Experimental Medicine, University of Perugia, Perugia 06132, Italy.

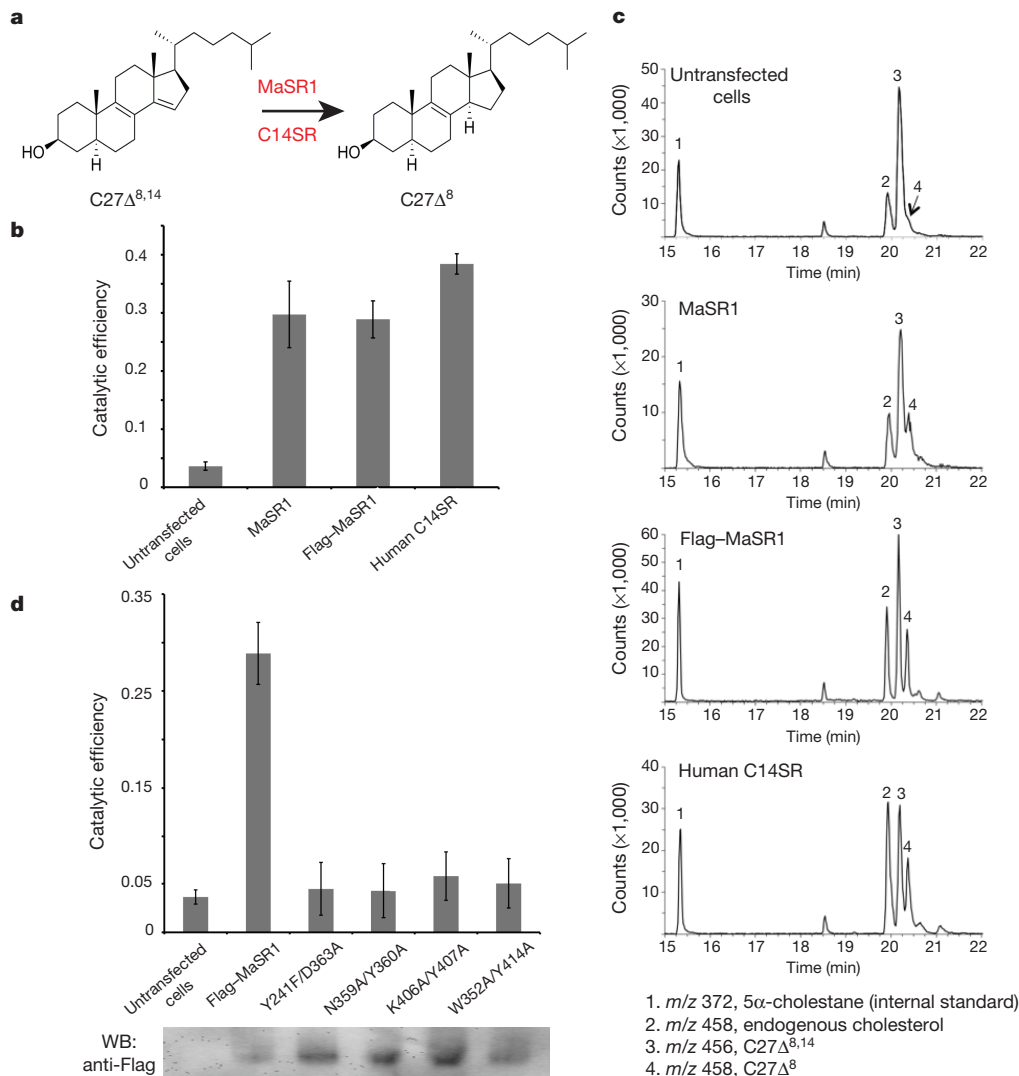


**Figure 1** |  $\Delta^{14}$ -reductase activity of MaSR1. **a**, Reaction catalysed by transfected human C14SR or MaSR1 in which 5 $\alpha$ -cholesta-8,14-dien-3 $\beta$ -ol (C27 $\Delta^{8,14}$ ) is converted to 5 $\alpha$ -cholesta-8-en-3 $\beta$ -ol (C27 $\Delta^8$ ). **b**, The average catalytic efficiency in two different experiments (calculated as the integrated gas chromatography–mass spectrometry (GC–MS) chromatogram peak area ratio C27 $\Delta^8$ /(C27 $\Delta^{8,14}$  + C27 $\Delta^8$ )) of untransfected HEK293 cells and cells transfected with MaSR1, Flag–MaSR1 and human C14SR is 3.6%, 29.7%, 28.9% and 38.4%, respectively. The thin black lines show the spread between the two individual measurements **c**, GC–MS chromatograms of  $\Delta^{14}$ -sterol reductase

assay. Peak 1, mass to charge ratio ( $m/z$ ) 372, 5 $\alpha$ -cholestane (an internal standard); peak 2,  $m/z$  458, endogenous cholesterol; peak 3,  $m/z$  456, C27 $\Delta^{8,14}$ ; peak 4,  $m/z$  458, C27 $\Delta^8$ . The reduced products (peak 4) were detected in MaSR1, Flag–MaSR1 and C14SR but little in untransfected cells. **d**, The catalytic efficiency of Flag–MaSR1 mutants. All mutants expressed by anti-Flag western blot (WB) detection. The plotted values in the grey bars are the average of two different experiments. The thin black lines show the spread between the measurements.

with the substrate. In our structure, the absence of a sterol substrate probably fails to coordinate the nicotinamide ring and hence causes it to be disordered. By contrast, the other half of the NADPH molecule is well defined in the electron density and stabilized by a hydrogen bond from the centrally located Tyr 414 of  $\alpha 2$  (Fig. 3a). The remainder of the NADPH pocket is lined with residues from TM9 and TM10 as well as two residues from TM8 (Fig. 3a). The NADPH pocket extends further around TM10 providing enough space to house the nicotinamide-ribose moiety of NADPH (Extended Data Fig. 6c). We mutated several residues in the NADPH binding pocket of MaSR1 (Extended Data Fig. 2). These mutations led to the loss of catalytic activity, as judged by the human  $\Delta^{14}$ -sterol reductase activity assay (Fig. 1d) and by the Erg24 complementation assay in yeast (Extended Data Fig. 3, lanes 4, 6 and 7).

The working principle of reductases is to bring the nicotinamide of NADPH into close proximity to the substrate, leading to carbon–carbon

double bond reduction. Analogous to the catalytic pocket of soluble sterol 5 $\beta$ -reductase<sup>3</sup> (AKRID1, Protein Data Bank (PDB) accession number 3COT), bound to progesterone (Fig. 3b), the lipid-bilayer-facing cavity of MaSR1 is the likely candidate for the sterol binding pocket (Fig. 3c). Notably, the sterol binding pockets of both enzymes contain a ‘signature’ motif forming triangular hydrogen bonds that coordinate the  $\beta 3$  hydroxyl of either sterol or steroid; for MaSR1, this signature motif includes Tyr 241 bonded to Asp 363 (Fig. 3c) and for steroid 5 $\beta$ -reductase, Tyr 58 bonded to Glu 120 (Fig. 3b). The distance between Tyr 58 and Glu 120 (4.1 Å) in steroid 5 $\beta$ -reductase is similar to that of Tyr 241 and Asp 363 (3.9 Å) in MaSR1. The MaSR1 double mutant Y241F/D363A loses sterol reductase function in the human  $\Delta^{14}$ -sterol reductase activity assay (Fig. 1d) and the yeast Erg24 complementation assay (Extended Data Fig. 3, lane 5). For the putative sterol binding pocket, extensive hydrophobic contacts between the highly conserved Trp 274

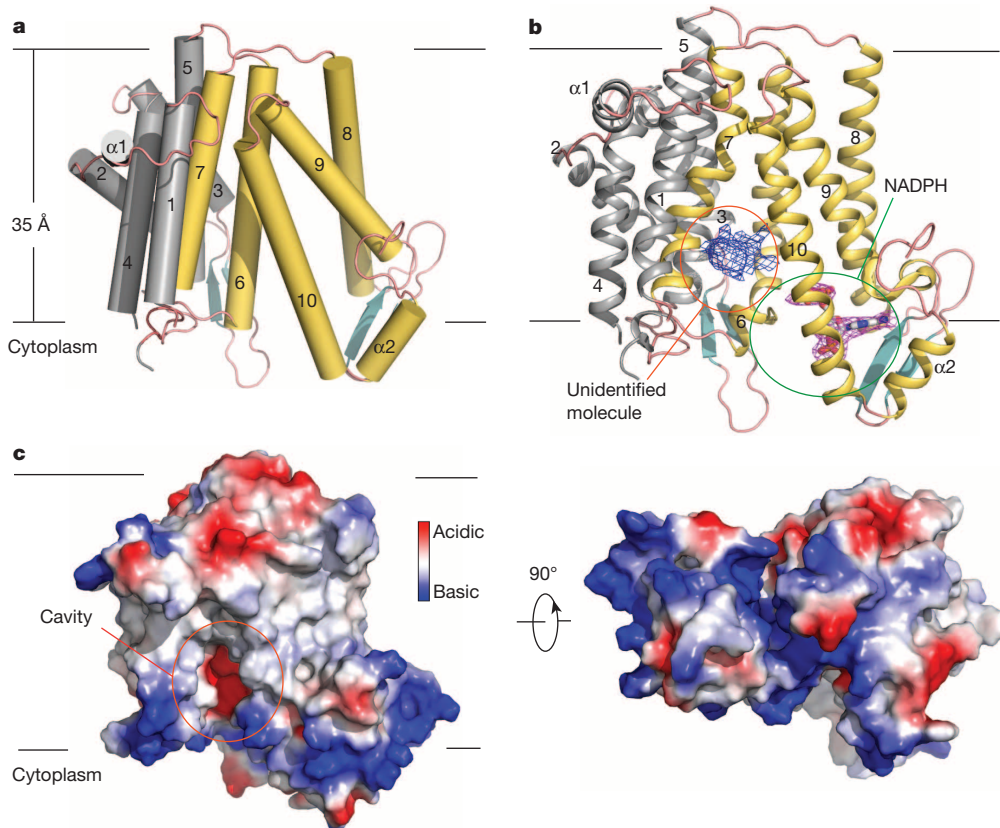


**Figure 2 | The molecular architecture of MaSR1.** **a**, Overall structure of MaSR1 viewed parallel to the membrane. The ten transmembrane segments are divided into an N-terminal half (TM1–5 and  $\alpha 1$ , grey) and a C-terminal half (TM6–10 and  $\alpha 2$ , yellow). The two black lines show the approximate location of the lipid bilayer. **b**, MaSR1 structure cartoon with NADPH shown by stick representation.  $2F_o - F_c$  map for an unidentified molecule (blue mesh) and simulated annealing (SA)-omit map ( $F_o - F_c$  densities) for NADPH (magenta mesh) both contoured at  $2\sigma$ . **c**, The cavity is indicated by an orange circle in an electrostatic surface representation. The right and left panels represent two perpendicular views.

and Tyr 387 residues enforce the interaction of TM7 and TM10 (Extended Data Fig. 6d). Notably, in each monomer of the crystallographic dimer there is the extra electron density of an unidentified molecule in front of the cavity (Figs 2b and 3c). Although the molecular identity of this density could not be unambiguously determined (maybe an endogenous molecule from *Escherichia coli* or the detergent used for

purification), it may represent a substrate for the putative sterol binding pocket. We modelled that two binding pockets bring the reducing end of NADPH into close proximity to the sterol (steroid) carbon-carbon double bond to be reduced (Fig. 3d), similar to the aldo-keto reductase (AKR) family of enzymes involved in human steroidogenesis<sup>20</sup> (for example, AKR1C3 and AKR1C2).

Owing to the high sequence homology with human LBR and human DHCR7, we generated structural models based on MaSR1 to highlight disease-related mutations (Fig. 4). The PHA/HEM-related mutations of LBR and the SLOS-related mutations of DHCR7 could be almost entirely mapped to the sterol reductase catalytic domain affecting the cofactor binding or sterol entry/binding sites. The similarities in pathogenesis between PHA/HEM and SLOS could therefore arise from a defect in sterol reduction.

Intriguingly, substrate recognition for sterol reductases is not very specific. MaSR1 could reduce the double bond of both C27 $\Delta$ <sup>8,14</sup> (Fig. 1b) and of the yeast sterol substrate ergosta-8,14-dien-ol (Extended Data Fig. 3). This is consistent with previous observations for LBR: it can reduce C27 $\Delta$ <sup>8,14</sup> (ref. 16); complement C14SR function in *C14SR*<sup>-/-</sup> (also known as *Tm7sf2*<sup>-/-</sup>) mice<sup>21</sup>; and also reduce different yeast sterol substrates<sup>9</sup>. Finally, our structure also provides insight into the function of LBR. A DALI search for structural homologues of MaSR1 shows

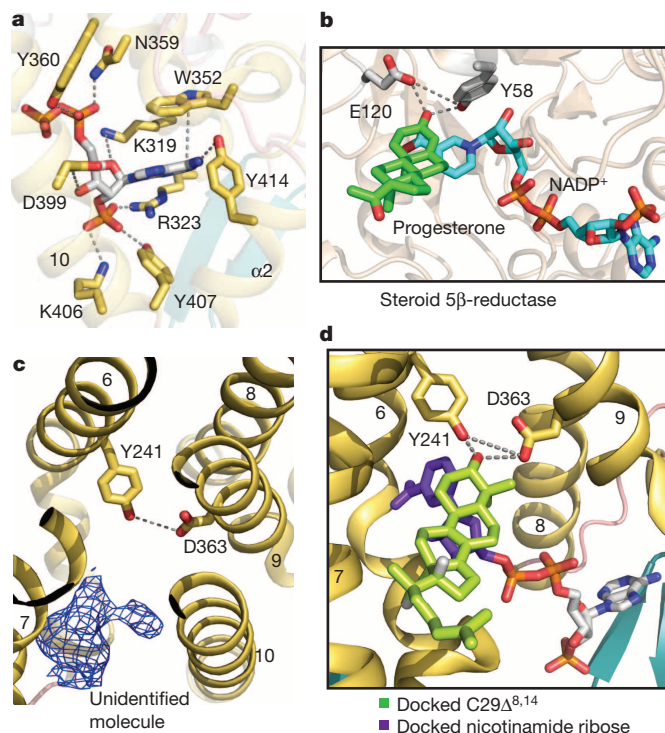


**Figure 3 | NADPH, putative sterol binding pockets and homology modelling with steroid 5 $\beta$ -reductase.** **a**, Close-up view of the NADPH binding pocket. NADPH is shown in stick representation with the phosphates in red. The interactions between NADPH and MaSR1 are indicated by dashed lines. **b**, Close-up view of the active pockets of steroid 5 $\beta$ -reductase (PDB accession number 3COT). Tyr 58 and Glu 120 clamp the  $\beta 3$  carbonyl oxygen of progesterone. **c**, The putative sterol binding site is accessible from the lipid bilayer. An unidentified ligand density is shown with  $2F_o - F_c$  map (blue mesh) at a  $2.5\sigma$ . **d**, Modelling of MaSR1 putative sterol binding pocket. On the basis of the active sites of steroid 5 $\beta$ -reductase, the missing nicotinamide-ribose moiety (purple) of NADPH was docked into the NADPH pocket and C29 $\Delta$ <sup>8,14</sup> (light green) modelled into the pocket of the MaSR1 structure.

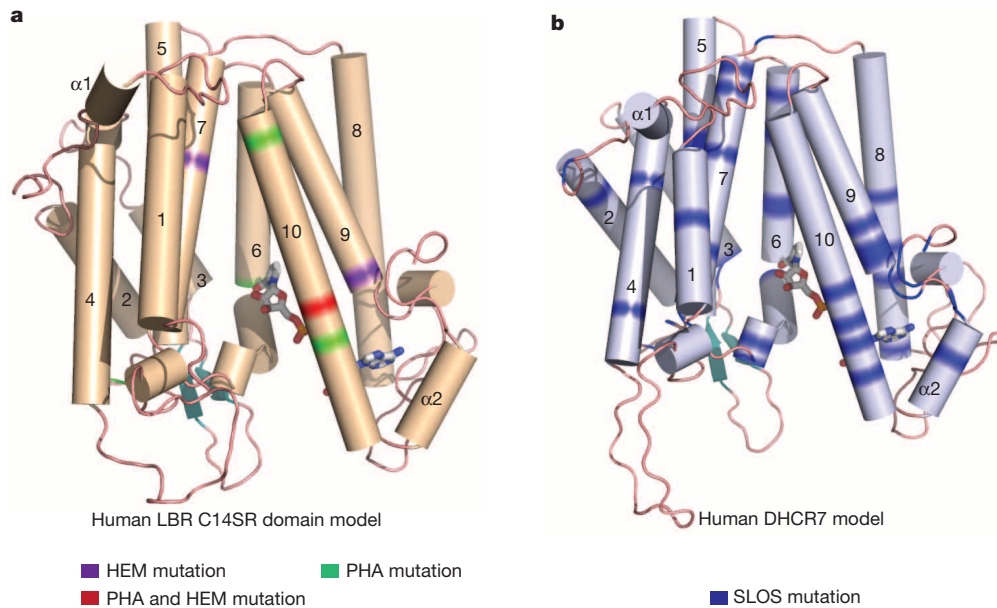


**Figure 4 | Models of human LBR and human DHCR7.** **a**, Human LBR model and the distribution of PHA and HEM mutations in green and purple, respectively. **b**, Human DHCR7 model and the distribution of SLOS mutations in blue. The cofactor NADPH (grey) is shown in stick representation.

no similar entry for the entire MaSR1 structure. However, it identified the membrane-embedded isoprenylcysteine carboxyl methyltransferase<sup>22</sup> (ICMT, PDB accession number 4A2N) as the closest entry for the TM6–10 segments of MaSR1 (Extended Data Fig. 7). The function of ICMT, which recognizes and then carboxymethylates the farnesylated cysteine of its substrate, points towards a similar role of the C14SR domain of LBR, which may recognize the farnesylated cysteine of either prelamin A or lamin B as the ligand<sup>23</sup>.

**Online Content** Methods, along with any additional Extended Data display items and Source Data, are available in the online version of the paper; references unique to these sections appear only in the online paper.

**Received 15 June; accepted 26 August 2014.**

**Published online 12 October 2014.**

- Porter, F. D. & Herman, G. E. Malformation syndromes caused by disorders of cholesterol synthesis. *J. Lipid Res.* **52**, 6–34 (2011).
- Worman, H. J., Yuan, J., Blobel, G. & Georgatos, S. D. A lamin B receptor in the nuclear envelope. *Proc. Natl Acad. Sci. USA* **85**, 8531–8534 (1988).
- Di Costanzo, L., Drury, J. E., Penning, T. M. & Christianson, D. W. Crystal structure of human liver  $\Delta^4$ -3-ketosteroid 5 $\beta$ -reductase (AKR1D1) and implications for substrate binding and catalysis. *J. Biol. Chem.* **283**, 16830–16839 (2008).
- Fahy, E. *et al.* A comprehensive classification system for lipids. *J. Lipid Res.* **46**, 839–862 (2005).
- Miller, W. L. & Bose, H. S. Early steps in steroidogenesis: intracellular cholesterol trafficking. *J. Lipid Res.* **52**, 2111–2135 (2011).
- Miller, W. L. Steroid hormone synthesis in mitochondria. *Mol. Cell. Endocrinol.* **379**, 62–73 (2013).
- Goldstein, J. L., DeBose-Boyd, R. A. & Brown, M. S. Protein sensors for membrane sterols. *Cell* **124**, 35–46 (2006).
- Olins, A. L., Rhodes, G., Welch, D. B., Zwerger, M. & Olins, D. E. Lamin B receptor: multi-tasking at the nuclear envelope. *Nucleus* **1**, 53–70 (2010).
- Silve, S., Dupuy, P. H., Ferrara, P. & Loison, G. Human lamin B receptor exhibits sterol C14-reductase activity in *Saccharomyces cerevisiae*. *Biochim. Biophys. Acta* **1392**, 233–244 (1998).
- Hoffmann, K. *et al.* Mutations in the gene encoding the lamin B receptor produce an altered nuclear morphology in granulocytes (Pelger–Huët anomaly). *Nature Genet.* **31**, 410–414 (2002).
- Waterham, H. R. *et al.* Autosomal recessive HEM/Greenberg skeletal dysplasia is caused by 3 $\beta$ -hydroxysterol  $\Delta^{14}$ -reductase deficiency due to mutations in the lamin B receptor gene. *Am. J. Hum. Genet.* **72**, 1013–1017 (2003).
- Porter, F. D. Smith–Lemli–Opitz syndrome: pathogenesis, diagnosis and management. *Eur. J. Hum. Genet.* **16**, 535–541 (2008).
- Herman, G. E. & Kratz, L. Disorders of sterol synthesis: beyond Smith–Lemli–Opitz syndrome. *Am. J. Med. Genet. C* **160**, 301–321 (2012).
- Shchukin, V. N., Khmelenina, V. N., Eshinimaev, B., Suzina, N. E. & Trotsenko, Yu. A. Primary characterization of dominant cell surface proteins of halotolerant

methanotroph *Methylomicrobium alcaliphilum* 20Z. *Microbiology* **80**, 595–605 (2011).

- Paik, Y. K., Trzaskos, J. M., Shafiee, A. & Gaylor, J. L. Microsomal enzymes of cholesterol biosynthesis from lanosterol. Characterization, solubilization, and partial purification of NADPH-dependent  $\Delta^{8,14}$ -steroid 14-reductase. *J. Biol. Chem.* **259**, 13413–13423 (1984).
- Roberti, R. *et al.* Cloning and expression of sterol  $\Delta^{14}$ -reductase from bovine liver. *Eur. J. Biochem.* **269**, 283–290 (2002).
- Bennati, A. M. *et al.* Sterol dependent regulation of human *TM7SF2* gene expression: role of the encoded 3 $\beta$ -hydroxysterol  $\Delta^{14}$ -reductase in human cholesterol biosynthesis. *Biochim. Biophys. Acta* **1761**, 677–685 (2006).
- von Heijne, G. Control of topology and mode of assembly of a polytopic membrane protein by positively charged residues. *Nature* **341**, 456–458 (1989).
- Kim, H., Melen, K., Osterberg, M. & von Heijne, G. A global topology map of the *Saccharomyces cerevisiae* membrane proteome. *Proc. Natl Acad. Sci. USA* **103**, 11142–11147 (2006).
- Miller, W. L. & Auchus, R. J. The molecular biology, biochemistry, and physiology of human steroidogenesis and its disorders. *Endocr. Rev.* **32**, 81–151 (2011).
- Bennati, A. M. *et al.* Disruption of the gene encoding 3 $\beta$ -hydroxysterol  $\Delta^{14}$ -reductase (*Tm7sf2*) in mice does not impair cholesterol biosynthesis. *FEBS J.* **275**, 5034–5047 (2008).
- Yang, J. *et al.* Mechanism of isoprenylcysteine carboxyl methylation from the crystal structure of the integral membrane methyltransferase ICMT. *Mol. Cell* **44**, 997–1004 (2011).
- Hennekes, H. & Nigg, E. A. The role of isoprenylation in membrane attachment of nuclear lamins. A single point mutation prevents proteolytic cleavage of the lamin A precursor and confers membrane binding properties. *J. Cell Sci.* **107**, 1019–1029 (1994).

**Acknowledgements** We thank W. Shi and H. Robinson at National Synchrotron Light Source (NSLS) beamline X29 and N. Sukumar at Advanced Photon Source (APS) beamline 24-ID-E for on-site assistance and J. Wang for support with the structure determination. We also thank L. Gatticchi and B. Sebastiani for assistance with the sterol reductase assays, and E. Coutavas, E. Deblor and H. Shi for constructive comments in manuscript preparation. The C27 $\Delta^{8,14}$  substrate was a gift to R.R. by G. Galli, University of Milano, Italy. This work was supported by funds from the Rockefeller University and the Howard Hughes Medical Institute. X.L. is supported by C.H. Li Memorial Scholar Fund fellowship of the Rockefeller University.

**Author Contributions** X.L. designed the research and performed structural biological studies; X.L. and R.R. performed sterol reductase activity assays; X.L., R.R. and G.B. contributed to data analysis and manuscript preparation; X.L. and G.B. wrote the manuscript.

**Author Information** Coordinates and structure factors for MaSR1 are deposited in the Protein Data Bank under accession code 4QUV. Reprints and permissions information is available at [www.nature.com/reprints](http://www.nature.com/reprints). The authors declare no competing financial interests. Readers are welcome to comment on the online version of the paper. Correspondence and requests for materials should be addressed to X.L. (xli05@rockefeller.edu) or G.B. (blobel@rockefeller.edu).

## METHODS

**Protein expression and purification.** We expressed a homologue of eukaryotic sterol reductases from the methanotrophic bacterium *Methylomicrobium alcaliphilum* 20Z (MaSR1, NCBI GI number: 503913803). Its cDNA was cloned into pET-21b (Novagen) with an N-terminal 8-His tag and expressed in *E. coli* C43(DE3) (Lucigen). The transformed cells were grown to an optical density of 1.0 at OD<sub>600</sub> and induced with 0.2 mM isopropyl- $\beta$ -D-thiogalactopyranoside (IPTG). Cells were disrupted using a French press with two passes at 15,000 p.s.i., in a buffer containing 25 mM Tris-Cl, pH 8.0, and 150 mM NaCl (buffer A). After low-speed centrifugation, the resulting supernatant was centrifuged at high speed to sediment a membrane fraction, which then was incubated in buffer A with 2% (w/v) *N*-dodecyl- $\beta$ -D-maltopyranoside (DDM, Anatrace) for 1 h at 4 °C. The lysate was centrifuged again and the supernatant was loaded onto Ni<sup>2+</sup>-NTA affinity column (Qiagen). After washing twice, the protein was eluted with 25 mM Tris-Cl, pH 8.0, 150 mM NaCl, 300 mM imidazole, and 0.1% DDM, and concentrated by centricon for subsequent gel filtration (Superdex-200, GE Healthcare) in buffer A with 0.4% (w/v) *N*-nonyl- $\beta$ -D-glucopyranoside ( $\beta$ -NG, Anatrace). The peak fraction was collected for crystallization. All mutations were generated using two-step PCR. Selenomethionine (SeMet)-labelled protein was purified similarly with the exception that 1 mM Tris [2-carboxyethyl] phosphine (TCEP) was included during the purification process.

**Crystallization.** Before crystallization, the protein solution was incubated with 2 mM NADPH (Sigma-Aldrich). Crystals were grown at 20 °C by the hanging-drop vapour-diffusion method. The crystals appeared after 5 days in the well buffer containing 0.1 M Tris-Cl pH 7.0, 0.2 M NH<sub>4</sub>Ac, 30% (v/v) pentaerythritol ethoxylate (15/4 EO/OH). DDM was added into crystallization buffer at 1% (v/v) final concentration to improve diffraction. SeMet-labelled protein was crystallized in the same buffer supplemented with 6 mM dithiothreitol (DTT). Platinum derivatives were obtained by soaking native crystals for 12 h in mother liquor plus 10 mg ml<sup>-1</sup> K<sub>2</sub>Pt(NO<sub>2</sub>)<sub>4</sub>. All crystals were directly flash-frozen in a cold nitrogen stream at 100 K.

**Data collection and structure determination.** The data were collected at National Synchrotron Light Source (NSLS) beamline X29. All data sets were processed using HKL2000 (ref. 24). Owing to the anisotropic diffraction properties, the outlier reflections were rejected based on extreme-value Wilson statistics using the program XTRIAGE<sup>25</sup> in the PHENIX package<sup>26</sup>. The anomalous signal in the SeMet-derivative data was further magnified with the local-scaling algorithm using the program SOLVE<sup>27</sup>. Then, the selenium sites were determined using the program SHELXD<sup>28</sup>. The identified sites were refined and the initial phases were generated in the program PHASER<sup>29</sup> with the single-wavelength anomalous dispersion experimental phasing module. Twofold NCS averaging along with solvent flattening and histogram matching was performed using DM<sup>30</sup>. The initial model was built in COOT<sup>31</sup> manually. The structure was refined with phenix.refine<sup>26</sup>. Model validation was performed with MolProbity<sup>32</sup>. Introduction of additional selenium anomalous scatterers by selective mutation and preparation of platinum derivatives confirmed the correctness of the atomic model.

The homology models of human LBR and human DHCR7 were generated by the program MODELLER<sup>33</sup> on the basis of the structure of MaSR1 in which the N-terminal regions (1–200 of LBR and 1–58 of DHCR7) were excluded because of low sequence conservation (Extended Data Fig. 2). All figures were generated using the program PyMOL (<http://www.pymol.org/>).

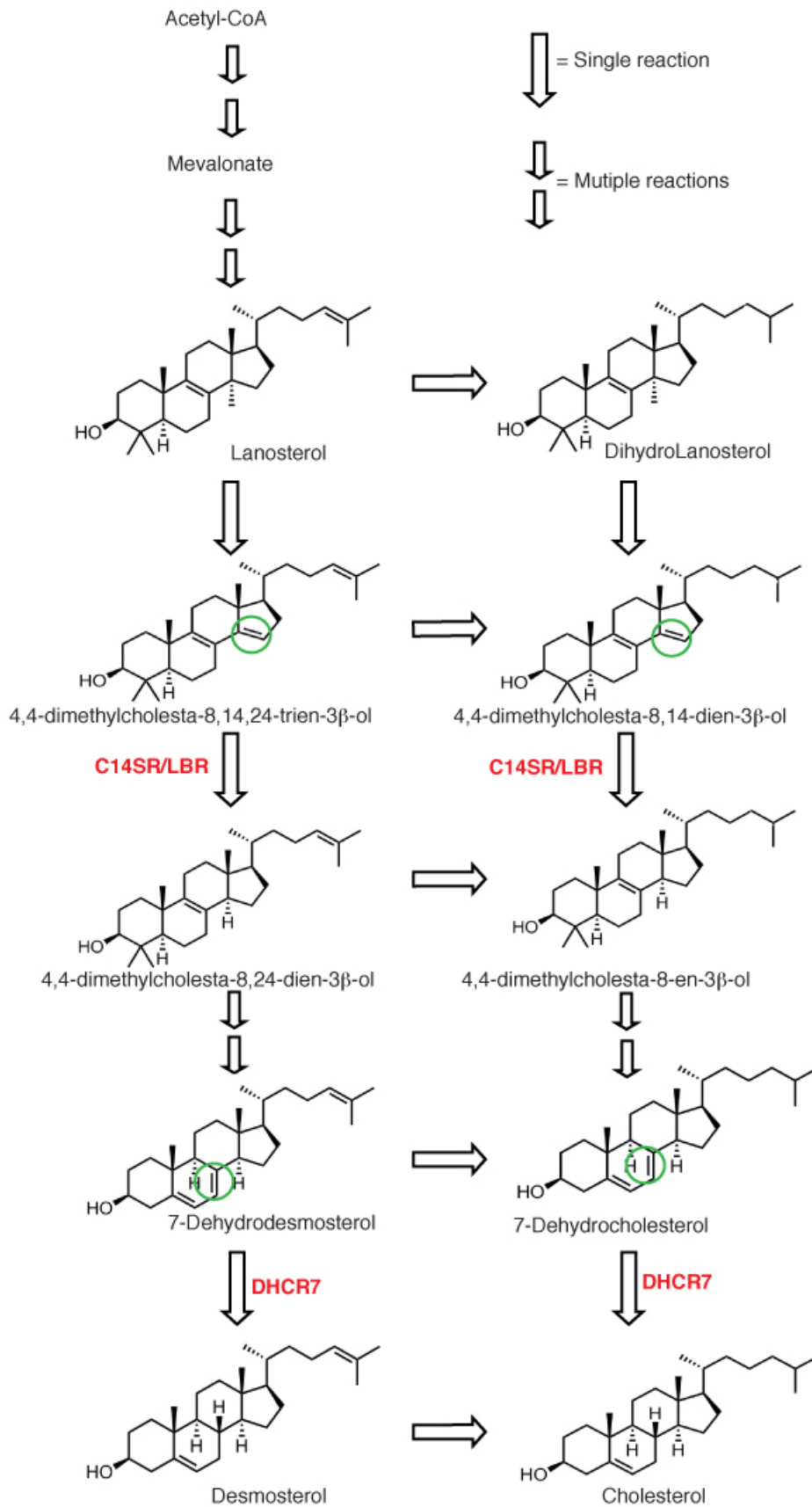
**Yeast reductase complementation assay.** Wild-type and mutant MaSR1 and ScErg24 were subcloned into the URA3 shuttle vector pCM190 (Euroscarf, Germany). The plasmids were introduced in Erg24-deficient *Saccharomyces cerevisiae* strain Y11164 (Euroscarf) by electroporation. A single colony was picked from a URA<sup>-</sup> selective plate. For the yeast rescue assay, the yeast was grown on URA<sup>-</sup> plates either in the absence or the presence of sub-inhibitory concentrations of cycloheximide (20 ng ml<sup>-1</sup>) at 30 °C for 24 to 48 h. The results were confirmed by three independent experiments with different colonies.

**$\Delta^{14}$ -reductase assay.** The cDNA encoding human  $\Delta^{14}$ -sterol reductase (C14SR) was subcloned into pCMV-SPORT6 (Open Biosystems). Wild-type and mutant MaSR1

were subcloned into pEGFP-N1 (Clontech) without the EGFP tag. HEK293 cells were grown in a 5% CO<sub>2</sub> incubator at 37 °C in DMEM supplemented with 10% fetal bovine serum, 2 mM L-glutamine, 100 U ml<sup>-1</sup> penicillin and 0.1 mg ml<sup>-1</sup> streptomycin. Cells were cultured in 10-cm Petri dishes to 80% confluence and transfected with the plasmids, using Lipofectamine 2000 (Life Technologies). After 48 h, transfected cells were recovered and the washed cell pellet was resuspended in PBS containing complete protease inhibitor cocktail (Sigma-Aldrich). Cells were lysed by sonication three times for 10 s on ice. After low-speed centrifugation, the resulting supernatant was ultracentrifuged to sediment a membrane fraction. The isolated membrane fraction was resuspended in 10 mM KPO<sub>4</sub>/0.5 mM EDTA (pH 7.4) and frozen in aliquots for further analyses. Protein concentration was determined by Bradford method, using bovine serum albumin as a standard. Proteins of the membrane fraction were separated by SDS-PAGE, blotted on PVDF and probed with mouse monoclonal anti-Flag M2 (Sigma-Aldrich) and peroxidase-conjugated goat anti-mouse (Santa Cruz). The protein was detected using Super Signal West Pico Chemiluminescent Substrate (Pierce).

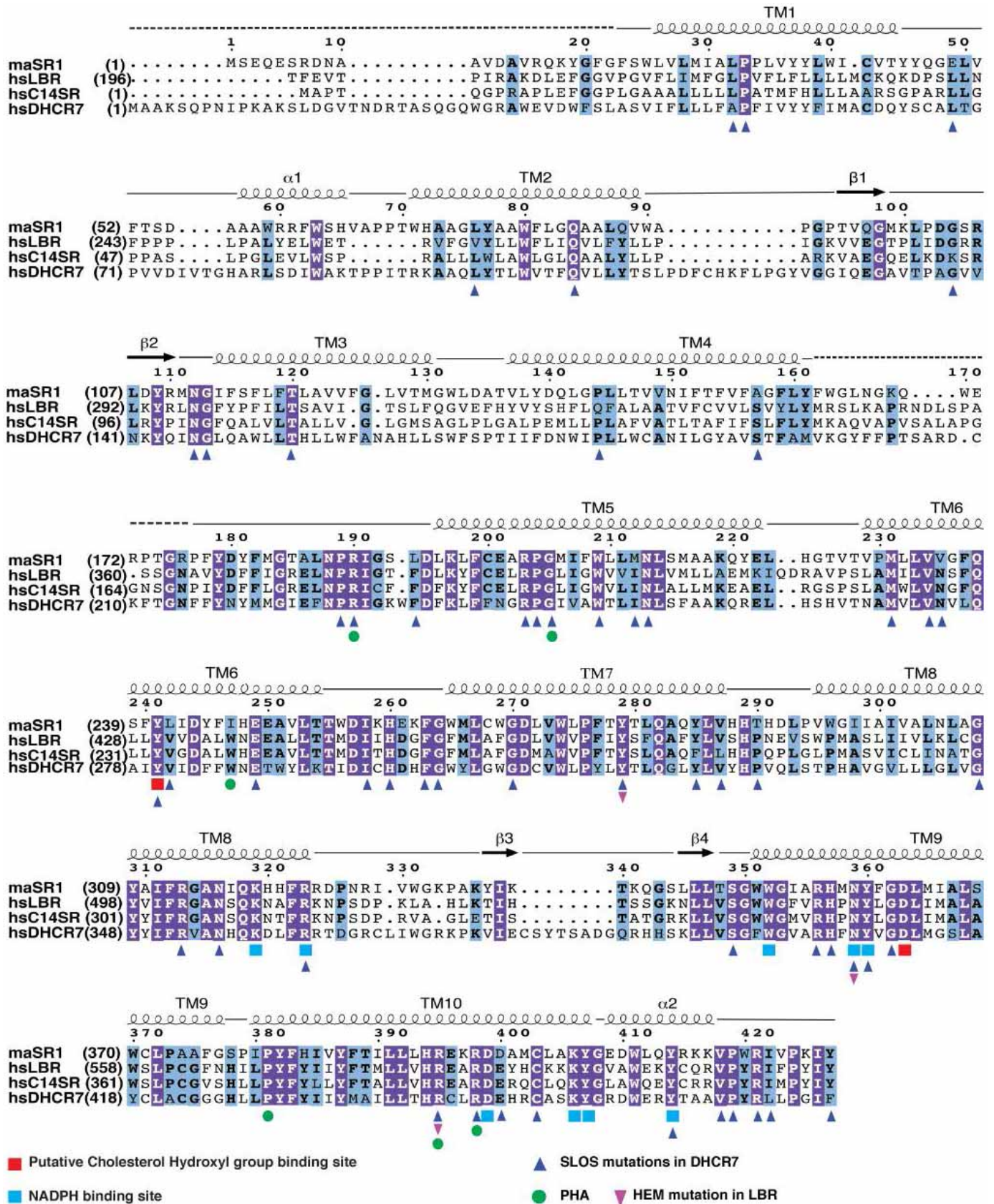
$\Delta^{14}$ -reductase activity was assayed in the membrane fractions obtained from transfected cells (0.25 mg protein per assay) using 5 $\alpha$ -cholesta-8,14-dien-3 $\beta$ -ol (C27 $\Delta^{8,14}$ ) as a substrate<sup>15–17</sup>. After the addition of 5 $\alpha$ -cholesta-8,14-dien-3 $\beta$ -ol (5  $\mu$ g) as an internal standard, sterols were extracted with petroleum ether, desiccated under nitrogen stream and converted to trimethylsilyl derivatives using N,O-Bis(trimethylsilyl) trifluoroacetamide (BSTFA) and pyridine (1:1, v/v). Gas chromatography–mass spectrometry (GC–MS) analysis was performed in multiple ion detection mode using a Varian GC-MS 2000 apparatus with a Varian CP-Sil8 CB low bleed capillary column. The trimethylsilylation of sterol products yields a molecular mass increase of 72 Da. Sterol retention times were: 15.31 min, 5 $\alpha$ -cholesta-8,14-dien-3 $\beta$ -ol (*m/z* 372); 19.90 min, cholesterol (*m/z* 458); 20.16 min, 5 $\alpha$ -cholesta-8,14-dien-3 $\beta$ -ol (C27 $\Delta^{8,14}$ , *m/z* 456); 20.34 min, 5 $\alpha$ -cholesta-8-en-3 $\beta$ -ol (C27 $\Delta^8$ , *m/z* 458).  $\Delta^{14}$ -reductase catalytic efficiency is calculated as the peak area ratio C27 $\Delta^8$ /(C27 $\Delta^{8,14}$  + C27 $\Delta^8$ ). The C27 $\Delta^8$  sterol was undetectable at zero incubation time.

24. Otwinowski, Z. & Minor, W. Processing of X-ray diffraction data collected in oscillation mode. *Methods Enzymol.* **276**, 307–326 (1997).
25. Zwart, P. H., Grosse-Kunstleve, R. W. & Adams, P. D. Xtriage and Fest: automatic assessment of X-ray data and substructure structure factor estimation. *CCP4 Newsletter* **43**, 27 (2005).
26. Adams, P. D. et al. PHENIX: a comprehensive Python-based system for macromolecular structure solution. *Acta Crystallogr. D* **66**, 213–221 (2010).
27. Terwilliger, T. C. & Berendzen, J. Automated MAD and MIR structure solution. *Acta Crystallogr. D* **55**, 849–861 (1999).
28. Schneider, T. R. & Sheldrick, G. M. Substructure solution with SHELXD. *Acta Crystallogr. D* **58**, 1772–1779 (2002).
29. McCoy, A. J. et al. Phaser crystallographic software. *J. Appl. Crystallogr.* **40**, 658–674 (2007).
30. Cowtan, K. dm: An automated procedure for phase improvement by density modification. *Joint CCP4 and ESF-EACBM Newsletter on Protein Crystallogr.* **31**, 34–38 (1994).
31. Emsley, P. & Cowtan, K. Coot: model-building tools for molecular graphics. *Acta Crystallogr. D* **60**, 2126–2132 (2004).
32. Chen, V. B. et al. MolProbity: all-atom structure validation for macromolecular crystallography. *Acta Crystallogr. D* **66**, 12–21 (2010).
33. Fiser, A. & Sali, A. Modeller: generation and refinement of homology-based protein structure models. *Methods Enzymol.* **374**, 461–491 (2003).
34. Thompson, J. D., Higgins, D. G. & Gibson, T. J. CLUSTAL W: improving the sensitivity of progressive multiple sequence alignment through sequence weighting, position-specific gap penalties and weight matrix choice. *Nucleic Acids Res.* **22**, 4673–4680 (1994).
35. Clayton, P. et al. Mutations causing Greenberg dysplasia but not Pelger anomaly uncouple enzymatic from structural functions of a nuclear membrane protein. *Nucleus* **1**, 354–366 (2010).
36. Holm, L. & Rosenstrom, P. Dali server: conservation mapping in 3D. *Nucleic Acids Res.* **38**, W545–W549 (2010).



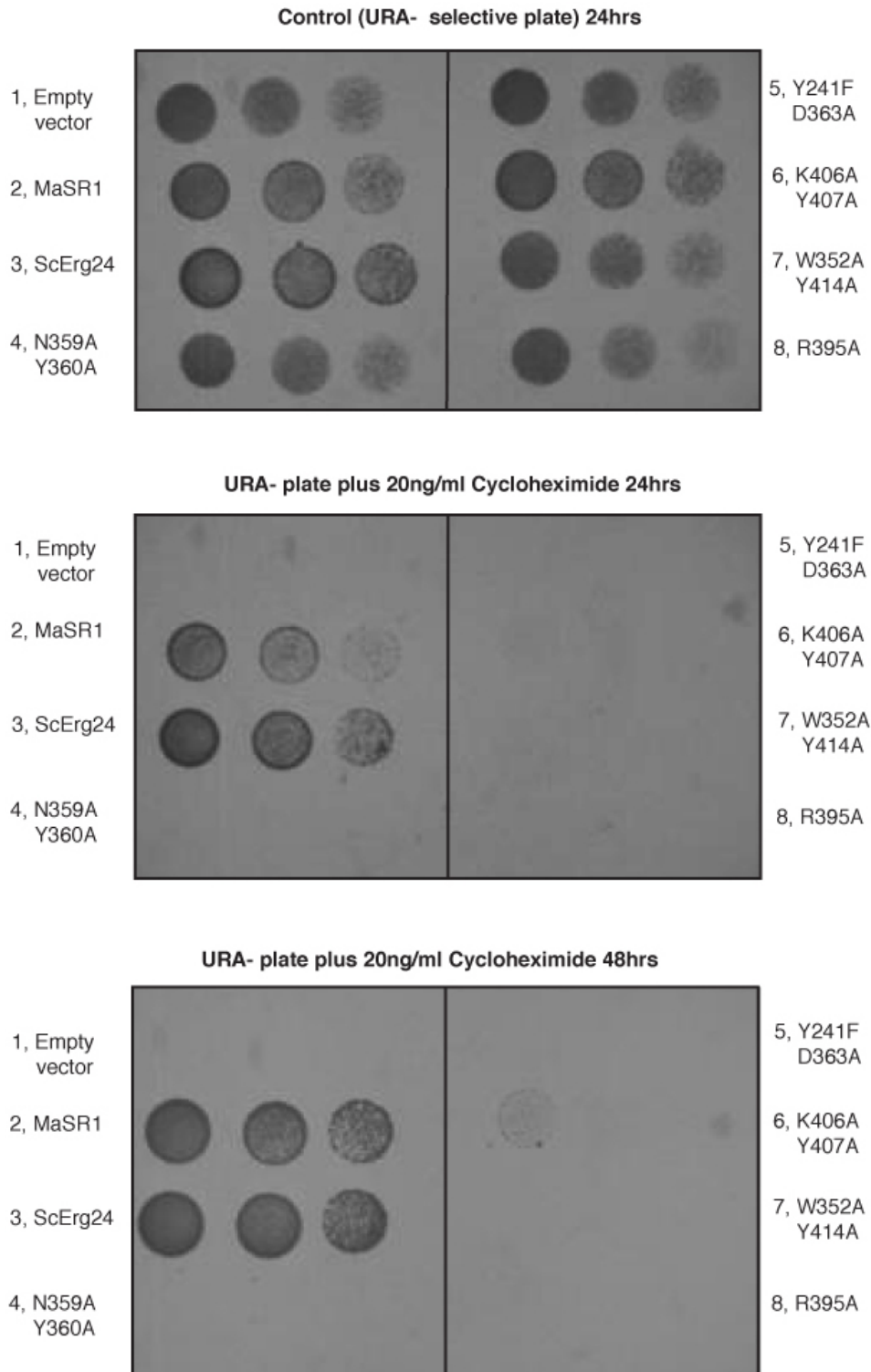
**Extended Data Figure 1 | Cholesterol biosynthesis pathway<sup>1</sup> and sterol reductase family.** Acetyl-CoA is the precursor for cholesterol biosynthesis. After several reactions, the intermediate lanosterol is synthesized. Conversion of lanosterol to cholesterol (Bloch pathway) involves many reactions, some of

which are catalysed by C14SR, LBR and DHCR7 (MaSR1 homologues, in red). C14SR, LBR and DHCR7 are homologues of NADPH-dependent reductases that catalyse the reduction of the sterol double bonds indicated in the green circles.



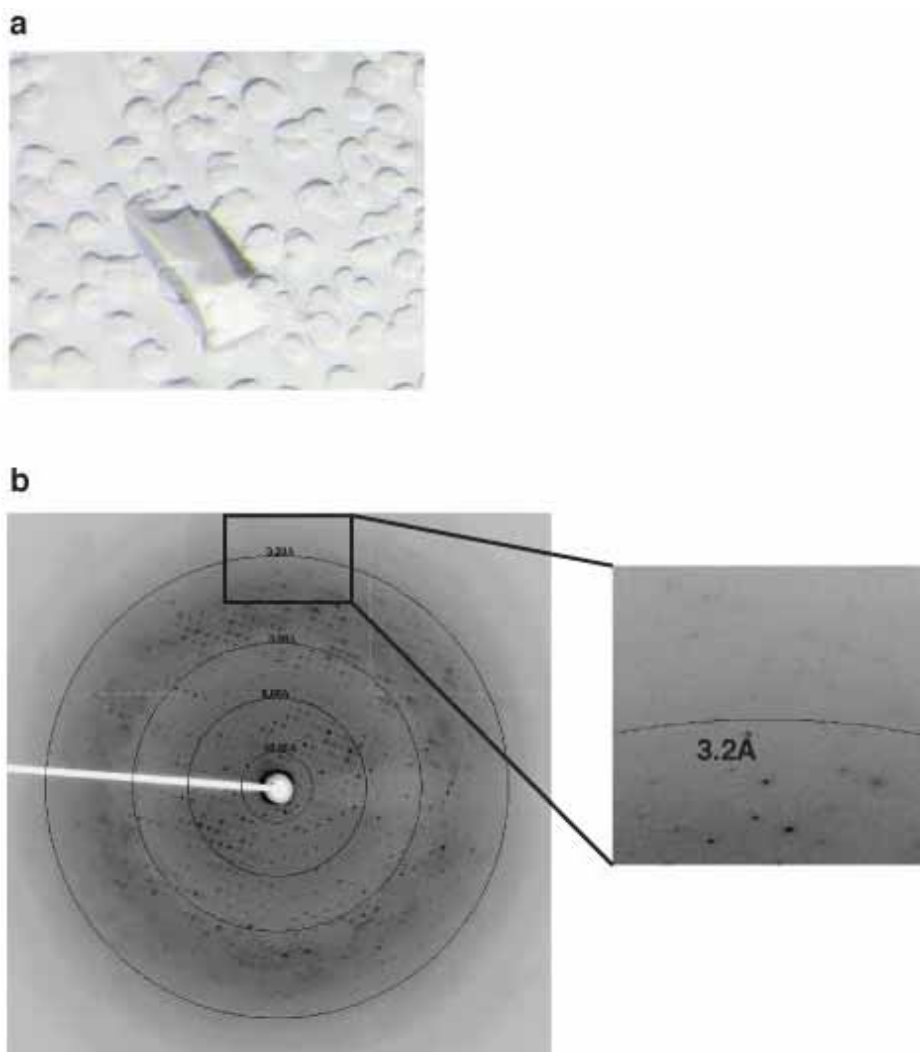
Extended Data Figure 2 | Sequence alignment of MaSR1 with human C14SR, DHCR7 and C-terminal domain of LBR. Secondary structural elements of MaSR1 are indicated above the sequences. Disordered regions in the MaSR1 structure are shown by a dashed line. Invariant amino acids are highlighted in blue (invariant in 3 of 4 proteins) and purple (invariant in all

proteins). Putative cholesterol hydroxyl group binding sites are highlighted in red, NADPH binding sites are highlighted in cyan. Human disease mutations are also highlighted by different symbols. Sequence alignment was carried out using ClustalW<sup>34</sup>.

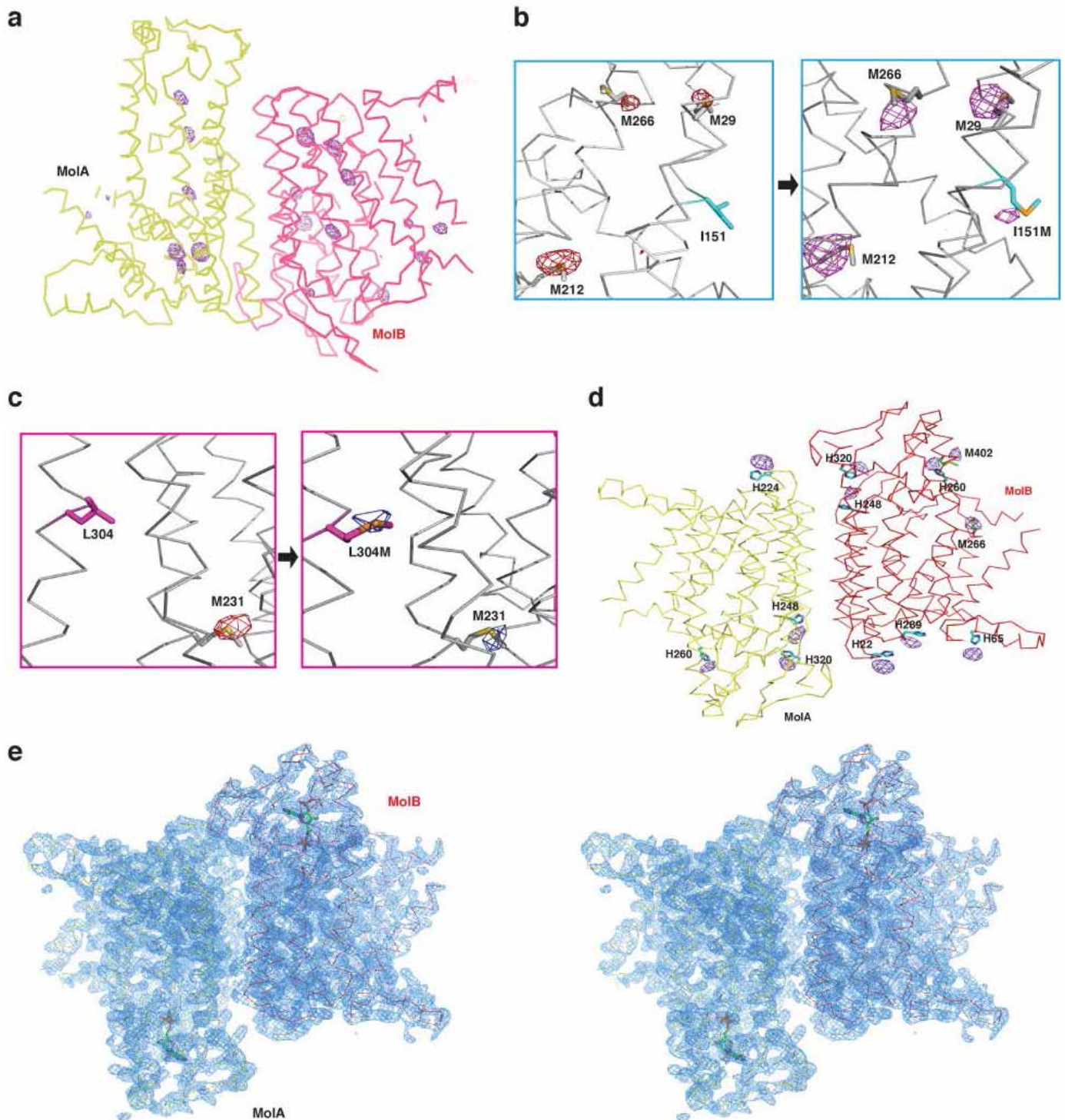


**Extended Data Figure 3 | Yeast complementation assay.** MaSR1 can rescue the growth of a *Saccharomyces cerevisiae*  $\Delta^{14}$ -sterol reductase Erg24 (yeast MaSR1 homologue) deletion strain ( $\Delta$ Erg24).  $\Delta$ Erg24 yeast expressing wild-type MaSR1, ScErg24 and mutated MaSR1 from a URA3 shuttle vector can grow under URA<sup>-</sup> selection (upper panel). Growth of yeast expressing MaSR1, ScErg24 and various mutated MaSR1 versions in the presence of sub-inhibitory

concentrations of cycloheximide (20 ng ml<sup>-1</sup>) for 24 to 48 h (lower panel). The yeast expressing MaSR1 or ScErg24 is able to grow in the presence of cycloheximide. R395A (lane 8) corresponds to R583Q in LBR which has been reported to lead to loss of activity in yeast<sup>35</sup>. Results are representative of three independent experiments.

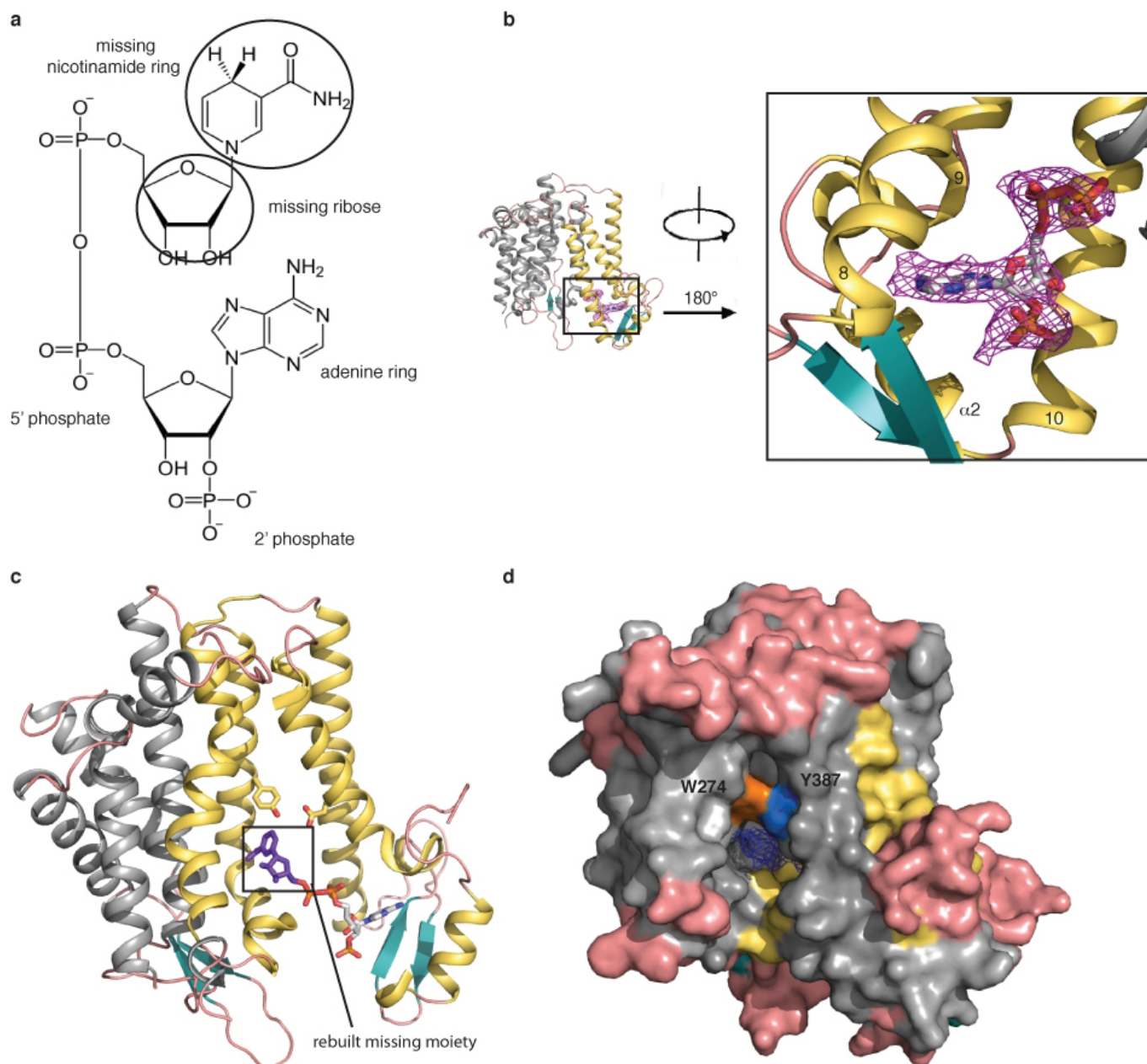


**Extended Data Figure 4 | MaSR1 crystal and X-ray diffraction image.** a, Photograph of MaSR1 crystal. b, A representative X-ray diffraction image of MaSR1 crystals with various resolution rings indicated by the circles.



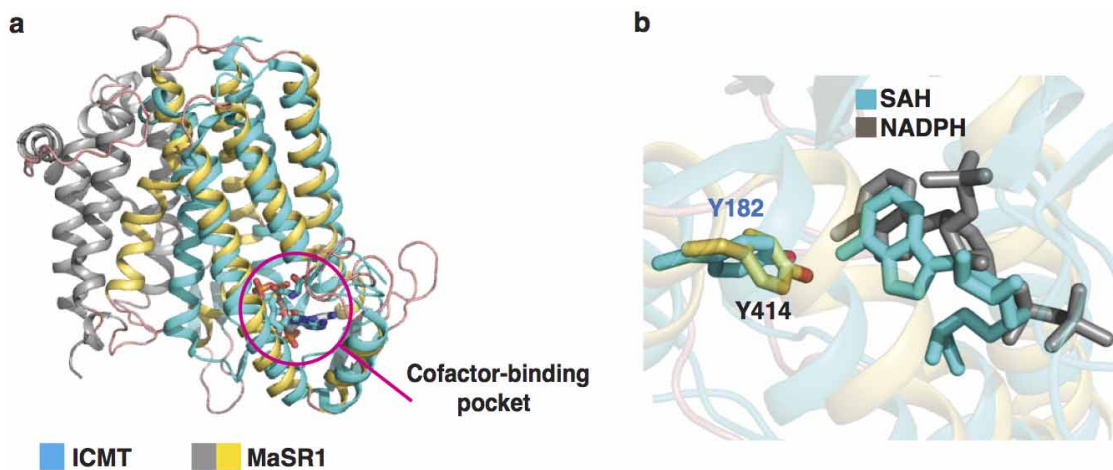
**Extended Data Figure 5 | Anomalous difference Fourier electron density.** **a**, Overview of the anomalous difference Fourier map for selenium atoms in an asymmetric unit. The electron density is contoured at  $4.5\sigma$  (purple mesh). Two molecules (MolA, molecule A; MolB, molecule B) were observed in each asymmetric unit. **b**, Examination of the atomic model in TM4 by selenium anomalous difference signals. Left panel shows wild-type SeMet anomalous difference signals; right panel shows mutated SeMet anomalous difference signals at  $3\sigma$  (purple mesh). **c**, Examination of the atomic model in TM8 by selenium anomalous difference signals. Left panel shows wild-type SeMet

anomalous difference signals, right panel shows mutated SeMet anomalous difference signals at  $3\sigma$  (blue mesh). **d**, A view of the anomalous difference Fourier map for platinum atoms in an asymmetric unit. The electron density is contoured at  $3\sigma$  (purple mesh). There are four platinum atoms binding to histidine residues in molecule A (yellow), but there are eight platinum atoms binding to six histidine and two methionine residues in molecule B (red). **e**, An overall view of the  $2F_o - F_c$  electron density, contoured at  $2\sigma$ , in one asymmetric unit.



**Extended Data Figure 6 | NADPH binding pocket and interaction between Trp 274 and Tyr 387 of MaSR1.** **a**, The structure of NADPH with the missing moiety in the MaSR1 structure indicated in the black circles. **b**, Overview of the NADPH-bound MaSR1. SA-omit map ( $F_o - F_c$  densities, magenta mesh) for NADPH contoured at  $2\sigma$ . The right panel is an enlargement of the left

panel (same orientation as Fig. 2a), rotated by  $180^\circ$ . **c**, The rebuilt missing moiety (purple) of NADPH in MaSR1. **d**, The surface representation shows Trp 274 (orange) and Tyr 387 (blue) located in the back of the sterol binding pocket.  $2F_o - F_c$  map for an unidentified ligand (blue mesh) contoured at  $2\sigma$ .



**Extended Data Figure 7 | Comparison of MaSR1 structure with ICMT structure.** **a**, A comparison of MaSR1 (grey and yellow) and ICMT<sup>22</sup> (cyan) structure with *S*-adenosyl-*L*-homocysteine (SAH) bound (PDB accession number 4A2N). DALI search<sup>36</sup> shows the closest entry (*Z*-score of 7.5) to MaSR1 is the structure of ICMT, consisting of 5 transmembrane helices, which had 193 C $\alpha$  atoms aligned to MaSR1 (TM6–10 and  $\alpha$ 2) with r.m.s.d. of 2.8 Å.

Both proteins have a similar cofactor binding pocket (magenta circle), although the sequence conservation is low. **b**, Comparison of NADPH and SAH binding pockets of MaSR1 (grey) and ICMT (cyan). The orientation of adenine–ribose moiety of SAH and NADPH is similar with respect to the coordinating tyrosine residues in the cofactor pockets of these two enzymes.

Extended Data Table 1 | Data collection and refinement statistics

	Native	Se-SAD
Wavelength (Å)	1.0750	0.9791
Space group	P1	P1
Unit cell (Å) (a,b,c; $\alpha,\beta,\gamma$ )	74.66, 74.62, 79.55; 66.00, 90.37, 86.86	74.81, 75.88, 80.27; 64.96, 89.95, 86.30
Resolution (Å)	50~2.74 (2.84~2.74)	50~3.3 (3.42~3.3)
R <sub>merge</sub> (%)	4.1 (41.5)	12.0 (64.6)
I/ $\sigma$ <sub>I</sub>	21.1 (1.4)	20.4 (1.7)
Completeness* (%)	74.8 (28.5)	83.0 (53.0)
Number of measured reflections	63,092	136,260
Number of unique reflections	30,595	19,876
Redundancy	2.1 (1.9)	6.9 (5.4)
Wilson B factor (Å <sup>2</sup> )	76.7	85.1
R <sub>work</sub> / R <sub>free</sub> (%)	23.29 / 28.37	
Molecules in ASU	2	
Number of atoms / B-factor:		
All atoms	6487 / 89.89	
Main chain	3128 / 89.13	
Side chain	3297 / 90.60	
Other entities	62 / 90.56	
Ramachandran plot (%):		
Favored/Allowed/Disallowed	90.8/9.2/0	
RMS-deviation in:		
Bond distances (Å)	0.013	
Bond angles (°)	1.646	

Values in parentheses are for the highest resolution shell. R<sub>free</sub> was calculated with 5% of the reflections selected in the thin shell. ASU, asymmetric unit.  
\* See Extended Data Table 2 of the native data completeness of each shell.

Extended Data Table 2 | Native data completeness of each shell

Resolution (Å)	Completeness (%)
50.00 – 6.09	95
6.09 – 4.83	98
4.83 – 4.23	97
4.23 – 3.84	98
3.84 – 3.56	97
3.56 – 3.35	89
3.35 – 3.19	73
3.19 – 3.05	60
3.05 – 2.93	49
2.93 – 2.83	37
2.83 – 2.74	28
Overall	74.8

**Extended Data Table 3 | Data collection statistics for the MaSR1 mutants I151M, L304M and Pt-derivatives**

Data Set	I151M	L304M	Pt-derivatives
Wavelength (Å)	0.9791	0.9791	1.0717
Space group	P1	P1	P1
Unit cell (Å) (a,b,c; $\alpha,\beta,\gamma$ )	74.77, 75.38, 79.75; 65.39,89.86,86.19	74.80, 76.81, 81.37; 63.69, 90.171, 86.67	78.63, 75.00, 74.48; 94.20, 65.88, 90.80
Resolution (Å) (outer shell)	50~3.2 (3.31~3.2)	50~4.3 (4.45~4.3)	50~3.51 (3.64~3.51)
R <sub>merge</sub> (%)	8.4 (53.8)	17.3 (81.5)	13.1 (79.3)
I/ $\sigma$ (outer shell)	24.0 (2.2)	7.3 (1.2)	12.8 (1.1)
Completeness (%)	86.9 (59.0)	81.2 (68.1)	82.2 (49.7)
Number of measured reflections	197,021	56,642	102,898
Number of unique reflections	22,484	8,813	15,845
Redundancy	8.9 (7.5)	6.4 (5.1)	6.5 (4.7)

Values in parentheses are for the highest resolution shell.